PAPER

Check for updates

Greatly enhanced photocatalytic activity by organic flexible piezoelectric PVDF induced spatial electric field†

Baoying Dai, [iD] [abc] Hengming Huang, [abc] Wei Wang, [iD] [d] Yukai Chen, [abc] Chunhua Lu,*[abc] Jiahui Kou,*[abc] Lianzhou Wang, [iD] [e] Fulei Wang[f] and Zhongzi Xu[abc]

Efficient charge separation accelerated by a spatial electric field is a vital factor for semiconductor photocatalysts to achieve high photocatalytic activity. In this work, poly(vinylidene fluoride) (PVDF) with piezoelectric effects was first introduced into a photocatalyst system to highly improve the photocatalytic efficiency. The results indicate that, in the presence of organic piezoelectric PVDF, the photocatalytic efficiency of a PVDF–TiO_2 film is improved by about 55%. The corresponding first-order reaction rate constant (k) value is increased 5.42 times. Moreover, photocatalytic activity enhancement is ascribed to the promotion effect of the spatial electric field on charge separation, which has been demonstrated by hydroxyl radical analysis. Furthermore, the results indicate that the spatial electric field of PVDF plays a generic enhancement role in the photocatalysis of both ultraviolet (UV)-light-responsive and visible-light-responsive photocatalysts. In a wider perspective, this work provides an efficient strategy, coupling solar energy and electric energy induced by organic flexible piezoelectric PVDF, to greatly enhance the photocatalytic performance.

1 Introduction

Photocatalysts could be employed to split water to generate clean green hydrogen, which could help to relieve the energy crisis.[1–6] Moreover, photocatalysts could be used to purify air and degrade organic waste in water into harmless substances.[7–11] Thus, photocatalysis is considered to be a promising and environmentally friendly technology, which has attracted growing attention around the world. However, the practical application of photocatalysts is still hampered by their low photocatalytic activity, which is mainly attributed to the high recombination rates of photogenerated electrons

and holes.[12] In recent decades, plenty of approaches have been proposed to promote charge separation, for instance, structural design, constructing p–n junctions, depositing cocatalysts and preparing nano-sized photocatalysts.[13–18] But the enhancement effect on photocatalytic performance is not good enough to meet the requirement of practical application. It is, therefore, imperative to explore more efficient strategies to greatly boost photocatalytic performance.

Currently, spatial electric fields have been proved to be helpful to enhance photocatalytic properties, it is possibly due to the fact that spatial electric fields facilitate the separation of photogenerated carriers.[19–21] In previous works, the employed spatial electric fields were all generated by inorganic ferroelectric powders, containing ZnO, $BaTiO_3$ and PMN-PT.[19–22] Although their photocatalytic activities have been much improved, piezoelectric photocatalytic composite powders are difficult to recycle in practical applications. Once mishandled, they will introduce secondary pollution into the environment.[23] Therefore, it is necessary to prepare piezoelectric photocatalytic composite films with great recycling ability and high photocatalytic activity. As we know, inorganic piezoelectric films are brittle, which greatly restricts their practical applications. Whereas, organic ferroelectrics exhibit great flexibility, being capable of sustaining larger strains compared with their inorganic counterparts.[24] From this point of view, organic ferroelectrics may have more advantages in using mechanical energy

[a] State Key Laboratory of Materials-Oriented Chemical Engineering, College of Materials Science and Engineering, Nanjing Tech University, Nanjing 210009, P. R. China. E-mail: chhlu@njtech.edu.cn, jhkou@njtech.edu.cn
[b] Jiangsu Collaborative Innovation Center for Advanced Inorganic Function Composites, Nanjing Tech University, Nanjing 210009, P. R. China
[c] Jiangsu National Synergetic Innovation Center for Advanced Materials (SICAM), Nanjing Tech University, Nanjing 210009, P. R. China
[d] School of Physics and Optoelectronic Engineering, Nanjing University of Information Science & Technology, Nanjing 210044, P. R. China
[e] Nanomaterials Center, School of Chemical Engineering and Australia Institute for Bioengineering and Nanotechnology, University of Queensland, Brisbane, Queensland 4072, Australia
[f] State Key Laboratory of Crystal Materials, Shandong University, Jinan, 250100, P.R. China
† Electronic supplementary information (ESI) available. See DOI: 10.1039/c7cy01638g

available in nature to generate spatial electric fields and boost photocatalytic performance. However, whether the spatial electric field generated by organic ferroelectrics is helpful to promote photocatalytic activity or not has not been reported yet. Hence, it is worthy to combine organic ferroelectrics with photocatalysts and investigate the impact of the spatial electric field of organic flexible piezoelectrics on photocatalysis.

PVDF, with a high piezoelectric coefficient among polymer ferroelectrics, has at least five crystal forms α, β, γ, δ and ϵ.[25–29] Among them, the β phase, with piezoelectric effects, can be readily formed by poling, high stretching, rapid thermal treatment, combining with nanoparticles, *etc.*[25–27] It has been extensively put into use in the energy conversion fields owing to its brilliant flexibility, non-toxicity and chemical stability.[25,28] Therefore, PVDF is an ideal candidate as a film substrate to combine with photocatalysts and generate a spatial electric field to enhance the photocatalytic performance.

In the present work, it is proposed that the spatial electric field generated by organic PVDF could greatly improve the photocatalytic activity. To verify this hypothesis, TiO_2, a typical UV light-responsive photocatalyst, was prepared and combined with PVDF. The degradation experiments of rhodamine B (RhB) over a PVDF–TiO_2 film were studied in the presence and absence of the spatial electric field of PVDF. Moreover, hydroxyl radical analysis was performed to demonstrate the promotion effect of the spatial electric field on charge separation. The generic improvement effect of the spatial electric field on photocatalysis was also manifested.

2 Experimental

2.1 Materials

Tetrabutyl titanate (Ti(OC$_4$H$_9$)$_4$, 98.0%, Shanghai Lingfeng Chemical Reagent CO., Ltd.) and ethanol (C$_2$H$_5$OH, 99.7%, Sinopharm Chemical Reagent Co., Ltd.) were employed to synthesize TiO_2 nanoparticles. Poly(dimethylsiloxane) ((C$_2$H$_6$-OSi)$_n$, PDMS, Sylgard 184, Dow Corning) and its curing agent, as well as poly(vinylidene fluoride) ((CH$_2$CF$_2$)$_n$, PVDF, MW ~543 000, Aldrich) were purchased to prepare photocatalytic film substrates. *N,N*-Dimethylformamide (C$_3$H$_7$NO, DMF, 99.5%, Sinopharm Chemical Reagent Co., Ltd.) and xylene (C$_8$H$_{10}$, 99.0%, Shanghai Lingfeng Chemical Reagent CO., Ltd.) were used as the solvents of PVDF and PDMS, respectively. All the reagents were of analytical grade and were utilized without further purification. Distilled water was used in the whole experiment.

2.2 Synthetic procedures

TiO_2 powders were synthesized *via* a hydrothermal method.[30] Tetrabutyl titanate was added dropwise into the mixture of distilled water and ethanol. After vigorous stirring for 30 min, the obtained mixture was transferred into a 100 mL homemade polytetrafluoroethylene (PPL)-lined stainless steel reactor and heated at 150 °C for 24 h. After cooling down to room temperature, the product was centrifuged and washed with distilled water and ethanol six times to remove all the undesired substances. Finally, the product was dried at 60 °C overnight in an oven.

1.0 g of PVDF powder was thoroughly dissolved in 9.0 g of DMF after continuous stirring for 3 h, forming a homogeneous transparent solution. Then 1.0 g of the as-prepared TiO_2 powder was added and the solution was stirred strongly for another 1 h. After that, the obtained mixture was scattered by ultrasonic waves for 10 min and coated onto glass slides (2.5 cm × 7.6 cm) with a coating machine. Lastly, the coated product was cured at 60 °C in a vacuum oven for 2 h to fabricate the PVDF–TiO_2 film. It should be noted that TiO_2 powders not only act as photocatalysts, but also serve as nucleating agents to provide the PVDF substrate with high piezoelectric phase contents. Furthermore, the pure PVDF film was also prepared *via* the fabrication process of the PVDF–TiO_2 film without TiO_2 powders.

For comparison, PDMS, without piezoelectric effects, was selected as the film substrate as well to combine with TiO_2. The preparation process of the PDMS–TiO_2 film is similar to that of PVDF–TiO_2. 0.6 g of the curing agent of PDMS was first dispersed in 4.0 g of xylene by ultrasonic wave vibration for 10 min. Then 6.0 g PDMS was added and the mixture was stirred strongly for 30 min to form a homogeneous solution. Subsequently, 1.0 g of synthesized TiO_2 powder was added and the mixture was stirred vigorously for 1 h. To avoid TiO_2 agglomeration in the resins, ultrasonic wave vibration was introduced and maintained for 10 min. After that, the mixture was coated on glass slides (2.5 cm × 7.6 cm) with a coating machine and cured at 70 °C for 4 h in an oven. The pure PDMS film was fabricated as well to compare the structures and optical properties of TiO_2, PDMS and PDMS–TiO_2.

2.3 Structure and morphology characterization

The phase structure characterization of the as-synthesized powders and films was performed on a SmartLab thin-film diffractometer employing Cu Kα radiation (λ = 0.15406 nm). The Fourier transform infrared (FT-IR) spectra of the prepared samples were measured by the KBr pellet method with a V PerkinElmer Frontier infrared spectrometer. The chemical states of the prepared samples were determined by X-ray photoelectron spectroscopy (XPS) in an ESCALAB 250Xi with a monochromatic Al Kα source (hv = 1486.6 eV). All the binding energies were calibrated using the C 1s peak (BE = 284.8 eV) as the standard. Scanning electron microscopy (SEM) was performed with an S-4800 scanning electron analyzer with an accelerating voltage of 15 kV. Transmission electron microscopy (TEM) and high resolution transmission electron microscopy (HRTEM) images were obtained with a 200 kV Titan. The contact angles of the samples were measured under ambient conditions with a Contact Angle Analyzer (JGW-306). The sessile drop method was used to determine the contact angle. The UV-vis absorption spectra of the prepared samples were obtained using an ultraviolet-visible-near infrared 3101 spectrophotometer.

This journal is © The Royal Society of Chemistry 2017

Catal. Sci. Technol., 2017, 7, 5594–5601 | 5595

2.4 Piezoelectric property measurement

The piezoelectric potential output signals were collected with an oscilloscope (Tektronix, DMO3024). Firstly, Au was sprayed on the top and bottom surfaces of the photocatalytic composite film with an area of 1 cm^2. Then two copper conductive wires were used to connect the sprayed Au layers to the positive electrode and negative electrode of the oscilloscope, respectively. After that, the film was packaged in a zip-lock bag. Finally, the film was immersed in water in the presence of ultrasonic wave vibration and the piezoelectric potential output signals were recorded simultaneously.

2.5 Photocatalytic performance measurement

To estimate the photocatalytic activity of the prepared films and investigate the promotion effect of the spatial electric field on photocatalysis, a 15 W lamp (λ_{max} = 254 nm) was used as a UV light source for PVDF–TiO$_2$ and PDMS–TiO$_2$ films. The distance between the light source and reactor was about 20 cm. The ultrasonic wave vibration was introduced by an SK3300HP ultrasonic machine with a working frequency of 53 kHz and a consumption power of 180 W. The degradation experiments of RhB (12 mg L^{-1}, 100 mL) were conducted under ultrasonic wave vibration in the presence (U–L) and absence (U–NL) of UV light irradiation, respectively. As a contrast, an experiment was also carried out using magnetic stirring and UV light illumination (S–L). Prior to catalytic reaction, one piece of the thin film was immersed in RhB solution which was stirred for 1 h in the dark to establish the adsorption–desorption equilibrium. During all the catalytic process, any temperature rises were avoided by cooling ethanol circulation. In the testing process, 3 mL of sample solution was taken out every 30 min and analyzed by an UV-vis spectrometer. The dye concentration of RhB was measured at its maximum absorption peak, λ = 553 nm. The percentage of degradation is designated as C/C_0 (C and C_0 are the test and original concentrations of the measured dye solution, respectively). The photocatalytic stability of the PVDF–TiO$_2$ film was investigated under U–L.

2.6 Hydroxyl radical generation analysis

To further demonstrate the acceleration effect of the spatial electric field on charge separation, hydroxyl radical generation experiment was performed in a similar way to the photocatalytic reaction process. In the experiment, terephthalic acid (TA) solution (1 × 10^{-3} mol L^{-1}) with a concentration of sodium hydroxide (8 × 10^{-3} mol L^{-1}) replaced RhB. 2-Hydroxyterephthalic acid, a highly fluorescent compound, is the reaction product of hydroxyl radicals and TA. Therefore, the photoluminescence (PL) spectra of 2-hydroxyterephthalic acid were recorded using a Jobin Yvon FL3-221 fluorescence spectrophotometer every 30 min after the adsorption–desorption equilibrium was established under the excitation and emission wavelength of 315 and 425 nm, respectively. The relative emission intensity at 425 nm is designated as I/I_0,

where I and I_0 are the test and original PL intensity of the measured solution, respectively.

3 Results and discussion

3.1 Crystal structure and morphology

The phase structures of the prepared samples were first investigated. Fig. 1 shows the XRD patterns of the synthesized TiO$_2$ powders and composite film samples. The diffraction peaks of TiO$_2$ can be found at 25.4°, 38.0°, 48.1°, 54.8° and 62.9°, indexed to the (101), (004), (200), (105) and (204) planes of anatase TiO$_2$, respectively. The peaks are in good agreement with the reported values.[30] The obvious diffraction peak of the pure PVDF film at 20.1° proves that the α phase is the main structure, as displayed in the high-precision XRD pattern in Fig. 1(a). After combination with TiO$_2$, the diffraction peak of PVDF shifts to a larger degree, 20.6°, which indicates that the crystal structure of PVDF has been changed from the α phase to β phase, which is the piezoelectric phase.[24,31] It is ascribed to the existence of TiO$_2$ particles, which serve as nucleating agents providing a high β phase content. TiO$_2$ particle contribution to the piezoelectric phase formation of the PVDF substrate is further demonstrated by PFM, as depicted in Fig. S1.† Moreover, all the peaks of the pure TiO$_2$ powders are included in the XRD pattern of the PVDF–TiO$_2$ film, verifying that the crystal structure of TiO$_2$ has not been changed after combination with PVDF. The XRD pattern of the PDMS–TiO$_2$ film, as exhibited in Fig. 1(b), implies that the crystal structure of TiO$_2$ is still well maintained after combination with PDMS.

The morphologies of photocatalyst powders and films were studied to obtain a deep insight into the prepared samples. The SEM and TEM images of the TiO$_2$ sample are displayed in Fig. 2(a) and (b), respectively. The size of TiO$_2$ spherical particles is almost the same, about 10 nm. The crystallization of TiO$_2$ particles is quite good. The interplanar distance in TiO$_2$ particles is ca. 0.35 nm, corresponding to the spacing of the (101) plane, as described in the insert of Fig. 2(b). The top-view SEM images of PDMS–TiO$_2$ (c) and PVDF–TiO$_2$ (d) suggest that some TiO$_2$ particles are relatively uniformly distributed on the surfaces of the PDMS and PVDF substrates, respectively. The side-view SEM images, described
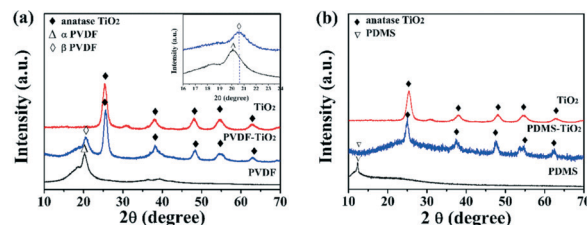
Fig. 1 XRD patterns of the as-synthesized TiO$_2$ powders, PVDF film and PVDF–TiO$_2$ film (a), the insert is the high-precision XRD patterns of the pure PVDF film and PVDF–TiO$_2$ film. XRD patterns of the TiO$_2$ powders, PDMS film and PDMS–TiO$_2$ film (b).

5596 | Catal. Sci. Technol., 2017, 7, 5594–5601

This journal is © The Royal Society of Chemistry 2017
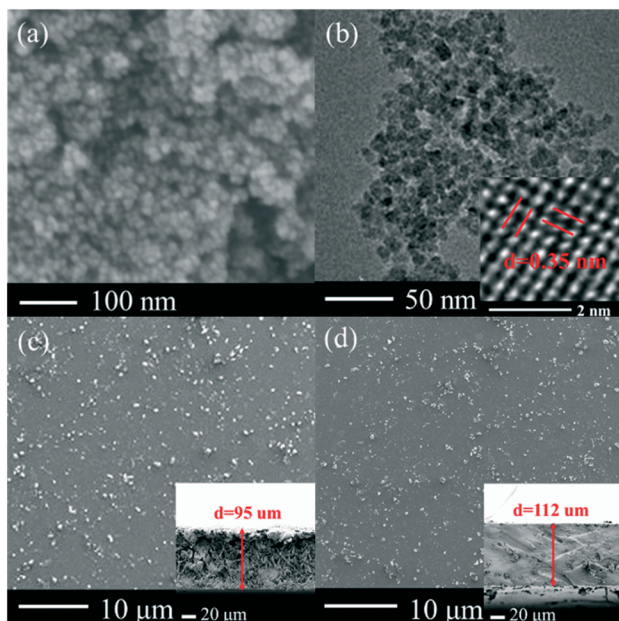
Fig. 2 SEM (a) and TEM (b) images of the as-prepared TiO$_2$ powders with low and high (insert) magnifications, top-view and side-view (insert) SEM images of the PDMS–TiO$_2$ film (c) and PVDF–TiO$_2$ film (d), respectively.

in the insert, of PDMS–TiO$_2$ and PVDF–TiO$_2$ indicate that the thickness of the prepared two films is similar, about 100 um.

3.2 Chemical structure and surface properties

The chemical structures of the prepared samples were investigated with FT-IR spectroscopy, as presented in Fig. 3. The strong peaks of TiO$_2$ are detected at about 3369 cm^{-1} and 1626 cm^{-1}, respectively. The peaks are associated with O–H stretching vibrations of water and Ti–OH, implying the presence of absorbed water on the surface of TiO$_2$ powders and crystal water in the catalyst.[32–35] These two peaks also appear in the spectra of PVDF–TiO$_2$ and PDMS–TiO$_2$, but not in the spectra of the pure PVDF and PDMS films. This reveals that TiO$_2$ powders are contained in both films. Furthermore, the obvious peak attributed to the β phase of PVDF at 1403 cm^{-1} (CH$_2$ bending) is clearly exhibited in the FT-IR spectrum of PVDF–TiO$_2$, but not in that of the pure PVDF film.[25] This once again demonstrates that the piezoelectric phase of PVDF
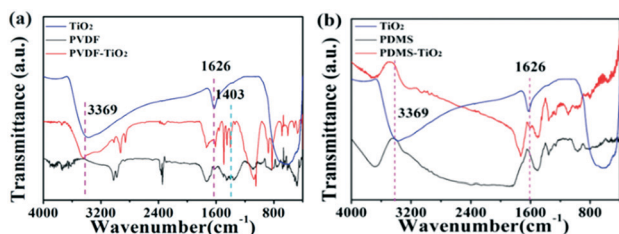
is formed in the PVDF–TiO$_2$ film, verifying the piezoelectric properties of the PVDF–TiO$_2$ film.

Surface wettability depends on the chemical composition, surface free energy and surface morphology of materials.[36–38] Therefore, to further demonstrate that some of the TiO$_2$ powders are exposed on the surfaces of the prepared films, it is necessary to characterize the wettability of the pure TiO$_2$ lamina and the prepared films. As shown in Fig. 4(a), the contact angle of a liquid droplet on the surface of the pure TiO$_2$ lamina is about 18°, indicating the great hydrophilic properties of prepared TiO$_2$. The contact angle of the pure PDMS film is 121° (Fig. 4(b)), and after mixing with TiO$_2$, the contact angle decreases to 112° (Fig.4(c)). Fig. 4(d) and (e) depict that the contact angles of PVDF and PVDF–TiO$_2$ films are 100° and 80°, respectively. The PVDF–TiO$_2$ and PDMS–TiO$_2$ films exhibit smaller contact angles than PVDF and PDMS, respectively. This result suggests that PVDF–TiO$_2$ and PDMS–TiO$_2$ possess better hydrophilic properties. This provides a powerful demonstration that some TiO$_2$ particles are exposed on the surfaces of PVDF–TiO$_2$ and PDMS–TiO$_2$ films.

3.3 Chemical states of TiO$_2$

The elemental composition and surface chemical states of TiO$_2$ were analyzed by XPS. The acquired data are depicted in Fig. 5. The full survey spectrum, described in Fig. 5(a), contains C, Ti, and O element peaks. The sharp photoelectron peak of C 1s appearing at the binding energy of 284.6 eV is ascribed to adventitious hydrocarbon from the XPS instrument itself.[39] Fig. 5(b) and (c) display the high-resolution spectra of Ti 2p and O 1s, respectively. Two peaks located at 464.4 eV and 458.5 eV (Fig. 5(b)) are assigned to Ti 2p$_{1/2}$ and Ti 2p$_{3/2}$, respectively.[40] Furthermore, it manifests that the main valence of Ti in the prepared TiO$_2$ is +4 and Ti^{4+} is in tetrahedral coordination with oxygen.[41] As shown in Fig. 5(c), the O 1s peak is found at 529.7 eV, which is attributed to the lattice oxygen of TiO$_2$.[40]

Fig. 3 FT-IR spectra of the as-synthesized samples: TiO$_2$ powders, PVDF film and PVDF–TiO$_2$ film (a) and TiO$_2$ powders, PDMS film and PDMS–TiO$_2$ film (b).
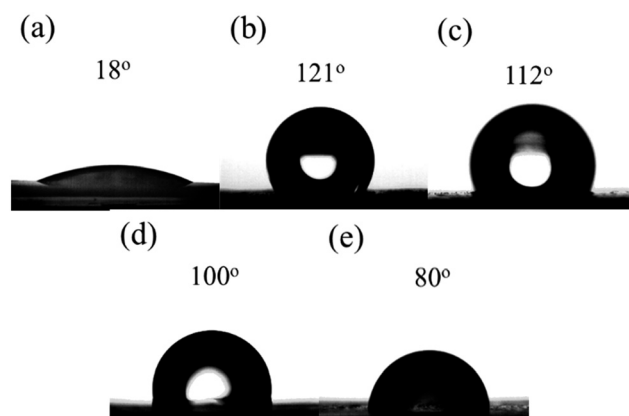
Fig. 4 The contact angles of the pressed TiO$_2$ powders (a), prepared PDMS film (b), PDMS–TiO$_2$ film (c), PVDF film (d) and PVDF–TiO$_2$ film (e).
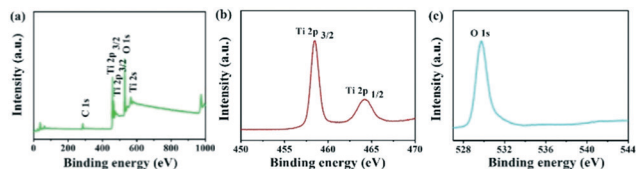
Fig. 5 The XPS spectra of the TiO_2 sample: survey spectrum (a), high-resolution spectra for Ti 2p (b) and O 1s (c).

3.4 Optical properties

UV-vis absorption spectra were analyzed to estimate the light absorption ability of the prepared samples. Fig. 6 depicts that TiO_2 powders show obvious photoabsorption at 400 nm, which corresponds to the band gap of 3.10 eV. It is consistent with the reported value.[39,40,42] Pure PVDF and PDMS films exhibit continuous light absorption in the wavelength range from 200 nm to 800 nm. This suggests that PVDF and PDMS, utilized as photocatalytic film substrates, do not influence the optical properties of photocatalysts. The result is further confirmed by the absorption edges of PVDF–TiO_2 and PDMS–TiO_2 films, which are similar to that of TiO_2 powders. Therefore, PVDF and PDMS substrates allow the prepared photocatalytic films to utilize enough UV light during the photocatalytic process.

3.5 Piezoelectric properties

To study the piezoelectric potential output of the prepared films during the photocatalytic reaction, the potential outputs of PDMS–TiO_2 and PVDF–TiO_2 films were recorded with the oscilloscope under ultrasonic wave vibration in water. The detected potential output signals are shown in Fig. 7. The weak potential signals (from −0.02 to +0.02 V displayed in the insert) introduced by the PDMS–TiO_2 film are ascribed to the instrument error of the oscilloscope, given both PDMS and TiO_2 without piezoelectric effects. Nevertheless, when the PVDF–TiO_2 film was irradiated with ultrasonic wave vibration, potential signals ranging from +4.0 V to −4.0 V were obtained. The big potential outputs are attributed to the enormous acoustic pressure caused by the cavitation effect, which deforms the film to generate piezoelectric potential.[19] Another decisive factor for the high potential outputs over the PVDF–TiO_2 film is the existence of TiO_2 inside PVDF. TiO_2 particles, contained in the PVDF–TiO_2 film, act as stress concentration points when the PVDF–TiO_2 film is subjected
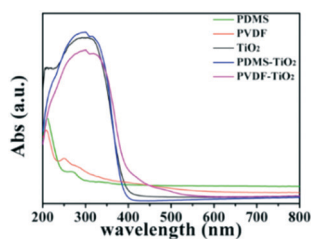
Fig. 7 Piezoelectric potential outputs of prepared PDMS–TiO_2 and PVDF–TiO_2 films under ultrasonic wave vibration in water. The insert is the magnified potential signals of the two films.

to acoustic pressure. Therefore, the local deformation of the PVDF segments is dramatically improved, and the piezoelectric potential output is greatly boosted. Furthermore, the irregularly changed potential output is due to the random direction of acoustic pressure.

3.6 Photocatalytic activity of PVDF–TiO_2 and PDMS–TiO_2

To investigate the influence of the spatial electric field generated by organic PVDF on the photocatalytic performance, the degradation experiments of RhB were conducted under U–L, S–L and U–NL, respectively. The corresponding first-order reaction rate constant (k) values were calculated. As depicted in Fig. 8(a), less than 20% of RhB are converted over PVDF–TiO_2 and PDMS–TiO_2 under U–NL in 4 h. The catalytic activities of the two films under U–L and S–L are much higher than that under U–NL. The order of photodegradation efficiencies of RhB over the two films is U–L-PVDF–TiO_2 (95%) > U–L-PDMS–TiO_2 (70%) > S–L-PDMS–TiO_2 (43%) ≈ S–L-PVDF–TiO_2 (38%). The similar RhB conversions over the two films under the S–L conditions indicate that the contents of TiO_2 powders exposed on the surfaces of both films are almost the same. Moreover, compared with S–L, U–L greatly accelerates the photocatalytic efficiency of PVDF–TiO_2 by more than 55%. The corresponding k value increased by 5.42 times from 0.12 h^{-1} to 0.65 h^{-1}. However, in the case of PDMS–TiO_2, U–L just improves its photocatalytic activity and k value by about 30% and 1.67 times (from 0.15 h^{-1} to 0.25 h^{-1}), much lower than 55% and 5.42, respectively. The result suggests that

Fig. 6 UV-vis absorption spectra of the fabricated samples: TiO_2 powders, PVDF, PDMS, PVDF–TiO_2 and PDMS–TiO_2 films.
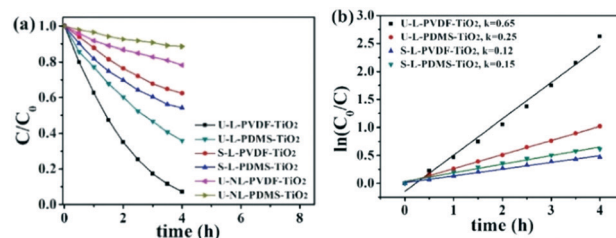
Fig. 8 The photocatalytic degradation curves of RhB (12 mg L^{-1}, 100 mL) over the PDMS–TiO_2 film and PVDF–TiO_2 film under U–L, S–L and U–NL, respectively (a), and variations of ln(C_0/C) versus light irradiation time of the PDMS–TiO_2 film and PVDF–TiO_2 film under U–L and S–L, respectively (b).

ultrasonic wave vibration boosts the photocatalysis of PVDF–TiO$_2$ and PDMS–TiO$_2$ in different ways.

3.7 Enhancement mechanism of the spatial electric field in photocatalysis

To make clear the reason for different enhancement effects of ultrasonic wave vibration on the photocatalysis of PVDF–TiO$_2$ and PDMS–TiO$_2$ films, further experiment was performed. As we know, the hydroxyl radical is the oxidation product of adsorbed water and photogenerated holes. Hydroxyl radicals could be trapped by TA, producing 2-hydroxyterephthalic acid, with high fluorescence properties. Therefore, higher PL intensity indicates more hydroxyl radicals trapped by TA and more effective photogenerated holes participating in the photocatalytic reaction. Thus, the PL intensity was employed as the probe to detect hydroxyl radicals and further to estimate the generation of photogenerated holes. Significant PL peaks over two films excited at 315 nm are observed (Fig. S2†). For better comparison, the relative emission intensities at 425 nm are shown in Fig. 9. The similar relative emission intensities over PVDF–TiO$_2$ (110) and PDMS–TiO$_2$ (40) under S–L imply the similar amounts of effective photogenerated holes of the two films, corresponding to the similar photocatalytic activities over the two films. Compared with S–L, U–L greatly improves the relative emission intensity of PVDF–TiO$_2$ (1120) by about 28 times. Nevertheless, the relative emission intensity of PDMS–TiO$_2$ (400) increased less, by about 4 times. This indicates that PVDF–TiO$_2$ generates much more effective photogenerated holes than PDMS–TiO$_2$ under U–L. Taking the similar contents of TiO$_2$ exposed on film surfaces, and the same light source and ultrasonic wave source for the above two films into account, the spatial electric field generated by PVDF–TiO$_2$ may be the reason for the big difference in the quantity of effective photogenerated holes, as well as the photocatalytic efficiencies, of PVDF–TiO$_2$ and PDMS–TiO$_2$ films under the U–L conditions.

In detail, it could be explained as follows: the photocatalytic composite film is irradiated with UV light and ultrasonic wave vibration, and enormous acoustic pressure deforms the film (Scheme 1(a)). As illustrated in Scheme 1(b), the spatial electric field is generated on the surfaces of the PVDF–TiO$_2$ film, owing to the piezoelectric effect of PVDF. Simultaneously, the photogenerated holes and electrons of TiO$_2$ directly transfer to the negative and positive potential surfaces
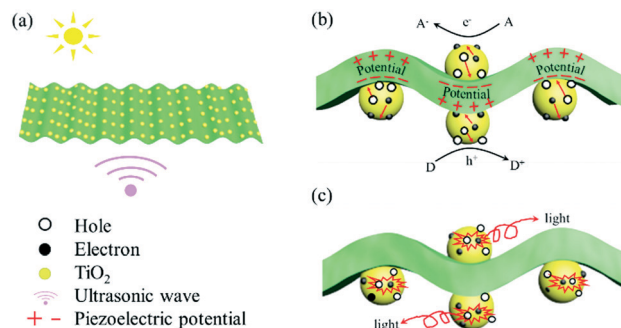
Scheme 1 The mechanism of the spatial electric field enhancing the photocatalytic performance. The photocatalytic film is irradiated with UV light and ultrasonic wave vibration (a). The PVDF–TiO$_2$ film deforms, piezoelectric potential is generated on its surface, and the charge separation of TiO$_2$ is accelerated (b). The PDMS–TiO$_2$ film deforms, no potential is introduced, and electrons and holes become recombined (c).

of the film, driven by the Coulomb force, to take part in the photocatalytic oxidation and reduction reactions, respectively. Thus, the charge separation is promoted, and more effective photogenerated electrons and holes participate in the photocatalytic reactions. As a result, a much higher photodegradation rate is obtained. While in the case of PDMS–TiO$_2$, without piezoelectric effects, even though the acoustic pressure deforms the PDMS–TiO$_2$, no spatial electric field is introduced on its surfaces in the presence of U–L. As illustrated in Scheme 1(c), the separation of photogenerated carriers is not accelerated. A great deal of photogenerated electrons and holes become recombined before taking part in the photocatalytic reactions. As a consequence, the photocatalytic performance of PDMS–TiO$_2$ is boosted poorly under the U–L conditions.

3.8 Photocatalytic stability of PVDF–TiO$_2$

The photocatalytic stability of photocatalysts is a crucial factor for their practical application, thus, the photocatalytic reusability of the PVDF–TiO$_2$ film was conducted under the U–L conditions. There is nearly no decrease in the catalytic activity of the film after five runs, as displayed in Fig. 10. This indicates the excellent photocatalytic stability of PVDF–TiO$_2$. Moreover, the degradation activity of RhB is maintained well over every run. This suggests that the PVDF–TiO$_2$ film possesses great piezoelectric stability and the spatial electric
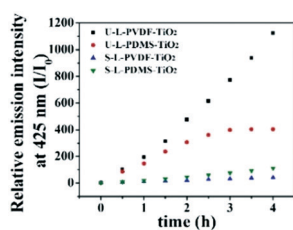
Fig. 9 Relative emission intensity of TA at 425 nm over the PDMS–TiO$_2$ film and PVDF–TiO$_2$ film under U–L and S–L, respectively.
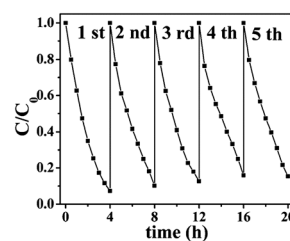
Fig. 10 The cyclic photocatalytic degradation curves of RhB (12 mg L^{-1}, 100 mL) catalysed by the PVDF–TiO$_2$ film under U–L.

field generated by PVDF accelerates the separation of the photogenerated carriers of TiO_2 throughout the whole photocatalytic process. Thus, organic flexible piezoelectric PVDF is a good candidate as a film substrate to generate the spatial electric field, greatly improve the photocatalytic activity and provide the composite film with good reusability.

3.9 Generic promotion effect of the spatial electric field of PVDF on photocatalysis

Furthermore, to investigate the generic promotion effect of the spatial electric field of PVDF on photocatalysis, UV-light-responsive photocatalyst $NaTiO_3$ and visible-light-responsive photocatalysts $BiVO_4$ and $g-C_3N_4$ were prepared and combined with PDMS and PVDF, respectively (Fig. S3–S5†). The degradation experiments of RhB over prepared films (Fig. S6 and S7†) verify that the spatial electric field of PVDF plays a generic enhancement role in the photocatalysis of both UV-light-responsive and visible-light-responsive photocatalysts. The results suggest that the enhancement effect of organic PVDF on photocatalysis is due to the nature promotion effect of the spatial electric field on charge separation rather than the particular properties of photocatalysts.

4 Conclusions

In summary, organic flexible PVDF with piezoelectric effects was firstly introduced into a photocatalyst system to greatly boost photocatalytic performance by promoting charge separation, which is demonstrated by hydroxyl radical generation analysis. The photocatalytic degradation rate of RhB over $PVDF–TiO_2$ is improved by about 55%. The corresponding reaction rate constant value is increased 5.42 times. Importantly, the results suggest that the spatial electric field introduced by organic piezoelectric PVDF exhibits a generic enhancement effect on photocatalysis. Thus, in a wider perspective, this work provides an efficient strategy to significantly enhance the photocatalytic activity by accelerating charge separation. Moreover, from the practical application point of view, compared with photocatalytic powders, the utilization of organic piezoelectric PVDF-based photocatalytic flexible composite films, with great recycling properties, could avoid introducing secondary pollution into the environment.

Conflicts of interest

There are no conflicts to declare.

Acknowledgements

References

1 J. Cheng, J. Feng and W. Pan, *ACS Appl. Mater. Interfaces*, 2015, **7**, 9638–9644.
2 M. Zhu, P. Chen and M. Liu, *ACS Nano*, 2011, **5**, 4529–4536.
3 F. Peng, Q. Zhou, D. Zhang, C. Lu, Y. Ni, J. Kou, J. Wang and Z. Xu, *Appl. Catal., B*, 2015, **165**, 419–427.
4 H. Liu, H. Hou, F. Gao, X. Yao and W. Yang, *ACS Appl. Mater. Interfaces*, 2016, **8**, 1929–1936.
5 A. Mukherji, B. Seger, G. Q. M. Lu and L. Wang, *ACS Nano*, 2011, **5**, 3483–3492.
6 G. Zhao, G. Liu, H. Pang, H. Liu, H. Zhang, K. Chang, X. Meng, X. Wang and J. Ye, *Small*, 2016, **12**, 6160–6166.
7 M. Liu, R. Inde, M. Nishikawa, X. Qiu, D. Atarashi, E. Sakai, Y. Nosaka, K. Hashimoto and M. Miyauchi, *ACS Nano*, 2014, **8**, 7229–7238.
8 T. K. Rahul and N. Sandhyarani, *Nanoscale*, 2015, 18259–18270.
9 D. Yang, J. Feng, L. Jiang, X. Wu, L. Sheng, Y. Jiang, T. Wei and Z. Fan, *Adv. Funct. Mater.*, 2015, **25**, 7080–7087.
10 Q. Li, X. Li, S. Wageh, A. A. Al-Ghamdi and J. Yu, *Adv. Energy Mater.*, 2015, **5**, 1500010.
11 W. Wang, M. O. Tade and Z. Shao, *Chem. Soc. Rev.*, 2015, **44**, 5371–5408.
12 W. L. Ong, M. Gao and G. W. Ho, *Nanoscale*, 2013, **5**, 11283.
13 H. Li, Y. Zhou, W. Tu, J. Ye and Z. Zou, *Adv. Funct. Mater.*, 2015, **25**, 998–1013.
14 N. Cheng, J. Tian, Q. Liu, C. Ge, A. H. Qusti, A. M. Asiri, A. O. Al-Youbi and X. Sun, *ACS Appl. Mater. Interfaces*, 2013, **5**, 6815–6819.
15 K. Li, S. Gao, Q. Wang, H. Xu, Z. Wang, B. Huang, Y. Dai and J. Lu, *ACS Appl. Mater. Interfaces*, 2015, **7**, 9023–9030.
16 G. Liu, G. Zhao, W. Zhou, Y. Liu, H. Pang, H. Zhang, D. Hao, X. Meng, P. Li, T. Kako and J. Ye, *Adv. Funct. Mater.*, 2016, **26**, 6822–6829.
17 L. Chen, Q. Gu, L. Hou, C. Zhang, Y. Lu, X. Wang and J. Long, *Catal. Sci. Technol.*, 2017, **7**, 2039–2049.
18 T. J. Wong, F. J. Lim, M. Gao, G. H. Lee and G. W. Ho, *Catal. Sci. Technol.*, 2013, **3**, 186–193.
19 H. Li, Y. Sang, S. Chang, X. Huang, Y. Zhang, R. Yang, H. Jiang, H. Liu and Z. L. Wang, *Nano Lett.*, 2015, **15**, 2372–2379.
20 X. Xue, W. Zang, P. Deng, Q. Wang, L. Xing, Y. Zhang and Z. L. Wang, *Nano Energy*, 2015, **13**, 414–422.
21 L. Wang, S. Liu, Z. Wang, Y. Zhou, Y. Qin and Z. L. Wang, *ACS Nano*, 2016, **10**, 2636–2643.
22 B. Dai, C. Lu, J. Kou, Z. Xu and F. Wang, *J. Alloys Compd.*, 2017, **696**, 988–995.

5600 | *Catal. Sci. Technol.*, 2017, **7**, 5594–5601

This journal is © The Royal Society of Chemistry 2017

23 B. Dai, L. Zhang, H. Huang, C. Lu, J. Kou and Z. Xu, *Appl. Surf. Sci.*, 2017, **403**, 9–14.

24 V. Bhavanasi, V. Kumar, K. Parida, J. Wang and P. S. Lee, *ACS Appl. Mater. Interfaces*, 2016, **8**, 521–529.

25 Y. Zhao, Q. Liao, G. Zhang, Z. Zhang, Q. Liang, X. Liao and Y. Zhang, *Nano Energy*, 2015, **11**, 719–727.

26 N. Jia, Q. Xing, G. Xia, J. Sun, R. Song and W. Huang, *Mater. Lett.*, 2015, **139**, 212–215.

27 Y. Kim, Y. Xie, X. Wen, S. Wang, S. J. Kim, H. Song and Z. L. Wang, *Nano Energy*, 2015, **14**, 77–86.

28 P. Talemi, M. Delaigue, P. Murphy and M. Fabretto, *ACS Appl. Mater. Interfaces*, 2015, **7**, 8465–8471.

29 V. Cauda, S. Stassi, K. Bejtka and G. Canavese, *ACS Appl. Mater. Interfaces*, 2013, **5**, 6430–6437.

30 G. Wang, *J. Mol. Catal. A: Chem.*, 2007, **274**, 185–191.

31 Z. Pi, J. Zhang, C. Wen, Z. Zhang and D. Wu, *Nano Energy*, 2014, 7, 33–41.

32 K. Kalantari, M. Kalbasi, M. Sohrabi and S. J. Royaee, *Ceram. Int.*, 2016, **42**, 14834–14842.

33 J. J. Murcia, M. C. Hidalgo, J. A. Navío, J. Araña and J. M. Doña-Rodríguez, *Appl. Catal., B*, 2013, **142–143**, 205–213.

34 H. Wang, C. Wang, B. Xiao, L. Zhao, J. Zhang, Y. Zhu and X. Guo, *Catal. Today*, 2016, **259**, 340–346.

35 G. S. Pozan and A. Kambur, *Appl. Catal., B*, 2013, **129**, 409–415.

36 B. Bharti, S. Kumar and R. Kumar, *Appl. Surf. Sci.*, 2016, **364**, 51–60.

37 M. Conradi and A. Kocijan, *Surf. Coat. Technol.*, 2016, **304**, 486–491.

38 E. György, A. P. Del Pino, A. Datcu, L. Duta, C. Logofatu, I. Iordache and A. Duta, *Ceram. Int.*, 2016, **42**, 16191–16197.

39 H. Wu, J. Ma, Y. Li, C. Zhang and H. He, *Appl. Catal., B*, 2014, **152–153**, 82–87.

40 B. Tian, R. Dong, J. Zhang, S. Bao, F. Yang and J. Zhang, *Appl. Catal., B*, 2014, **158–159**, 76–84.

41 J. Hou, C. Yang, Z. Wang, S. Jiao and H. Zhu, *Appl. Catal., B*, 2013, **129**, 333–341.

42 D. S. Kim and S. Kwak, *Appl. Catal., B*, 2007, **323**, 110–118.

This journal is © The Royal Society of Chemistry 2017

Catal. Sci. Technol., 2017, **7**, 5594–5601 | **5601**